Applied Mathematical Sciences, Vol. 8, 2014, no. 7, 345 - 353
HIKARI Ltd, www.m-hikari.com
http://dx.doi.org/10.12988/ams.2014.311619

Multitemporal Cloud Detection and Masking Using MODIS Data

Asmala Ahmad

Department of Industrial Computing
Faculty of Information and Communication Technology
Universiti Teknikal Malaysia Melaka
Hang Tuah Jaya, 76100 Durian Tunggal, Melaka, Malaysia

Shaun Quegan

Department of Applied Mathematics
School of Mathematics and Statistics
University of Sheffield
Sheffield, United Kingdom

Abstract

The aims of this study are to investigate the spectral properties of cloud and to carry out cloud detection and masking using MODIS (Moderate-resolution Imaging Spectroradiometer) data. To do this we make use of the spectrally rich satellite data provided by MODIS sensor, which is equipped with 36 bands ranging from visible to thermal wavelengths. Cloud detection and masking were first carried out individually using single date of MODIS data. Multitemporal cloud analysis was later carried out using MODIS data from 24 different dates from 2004 to 2005. The eastern parts of Malaysia were found to have more cloudy days than the western parts, in which consistence with the meteorological observations made by the Malaysian Meteorological Services.

Keywords: Cloud, Detection, Masking, MODIS, Multitemporal

1 Introduction

Retrieval of surface information using remote sensing satellite is commonly affected by cloud, which, if thick, can completely obscure the surface within the satellite field of view or, if thin, attenuate solar radiation both on the incident path and after reflection and scattering at the surface [2], [4]. This is particularly important over tropical regions where cloud is persistent. If not dealt properly, this could affect the accuracy of further common processing task such as land cover classification [1], [3], [5]. Generally, cloud detection tests can be categorised into four categories, i.e. brightness temperature test and brightness temperature difference test.

Brightness Temperature Test

The tests commonly performed using brightness temperature measurements are from 11 μm and 14 μm wavelengths. 11 μm measurement was initially used for partial coherence test [7]. The idea is that the absolute value of BT should be lower than surface area and the variability of brightness temperature for cloudy pixels should be higher than clear-sky pixels. This can be carried out by making use the standard deviation value of an array of pixels. Cloud pixels are indicated with standard deviation less than 0.4 K for equatorial regions. CO_2 absorption bands (near 14 μm) can be used to distinguish transparent clouds from opaque clouds and clear-sky. This test is effective for detecting thin cirrus clouds that are often missed by infrared and visible tests [12].

Brightness Temperature Difference Test

The frequently used brightness temperature difference tests are $BT(11) - BT(12)$ and $BT(11) - BT(3.9)$. $BT(11) - BT(12)$ test can be used to detect thin cloud (i.e. cirrus) because they are larger than that of clear-sky and thick cloud conditions [10]. $BT(11) - BT(3.9)$ test can be used to differentiate between cloud over land and water; its value over land is different from over water. For cloudy pixels over land, the long-wave minus shortwave brightness temperature (i.e. $BT(11) - BT(3.9)$) has a large negative value during the day for thick clouds. This is because much of the energy sensed by the satellite comes from the Earth's surface and atmosphere below the cloud, and the 3.9-μm channel's response to warm pixel temperatures is greater than it is at 11 μm, resulting in negative difference values during the day.

Reflectance Test

The frequently used reflectance tests are such as $R(0.66)$ and $R(1.38)$; $R(0.66)$ has been widely used in discriminating clouds from vegetated land due to the difference reflectance properties measured at 0.66 μm wavelength. $R(1.38)$ in day time can be used to detect the presence of high-level clouds, particularly thin cirrus, due to the strong water vapour absorption at that region [6].

2 Materials and Methods

The MODIS instrument is the primary payload attached to two satellites, Terra and Aqua. Terra was launched on December 18, 1999, and Aqua on May 4, 2002. The main advantage of MODIS data is that it offers a wide range of spectral bands. There are 36 spectral bands covering the visible, near infrared and thermal infrared ranges of the electromagnetic spectrum. The primary use and the corresponding spectral information for all bands are summarised in Table 1.

Table 1: Primary use and spectral information for MODIS bands [9].

Primary Use	Band	Band Range[1]	Bandwidth[2]	Spectral Radiance[3]	Central Wavelength[4]
Land/Cloud/Aerosols Boundaries	1	0.620 – 0.670	41.8	21.8	0.659
	2	0.841 -0. 876	39.4	24.7	0.865
Land/Cloud/Aerosols Properties	3	0.459 – 0.479	17.6	35.3	0.470
	4	0.545 – 0.565	19.7	29.0	0.555
	5	1.230 – 1.250	24.5	5.4	1.240
	6	1.628 – 1.652	29.7	7.3	1.640
	7	2.105 – 2.155	52.9	1.0	2.130
Ocean Colour/ Phytoplankton/ Biogeochemistry	8	0.405 – 0.420	11.8	44.9	0.415
	9	0.438 – 0.448	9.7	41.9	0.443
	10	0.483 – 0.493	10.6	32.1	0.490
	11	0.526 – 0.536	11.8	27.9	0.531
	12	0.546 – 0.556	10.4	21.0	0.565
	13	0.662 – 0.672	10.1	9.5	0.653
	14	0.673 – 0.683	11.4	8.7	0.681
	15	0.743 – 0.753	10.0	10.2	0.750
	16	0.862 – 0.877	15.5	6.2	0.865
Atmospheric Water Vapour	17	0.890 – 0.920	35.7	10.0	0.905
	18	0.931 – 0.941	13.7	3.6	0.936
	19	0.915 – 0.965	46.3	15.0	0.940
Surface/Cloud Temperature	20	3.660 - 3.840	36.4	0.45(300K)	3.750
	21	3.929 - 3.989	182.6	2.38(335K)	3.959
	22	3.929 - 3.989	85.7	0.67(300K)	3.959
	23	4.020 - 4.080	88.2	0.79(300K)	4.050
Atmospheric Temperature	24	4.433 - 4.498	87.8	0.17(250K)	4.465
	25	4.482 - 4.549	93.7	0.59(275K)	4.515
Cirrus Clouds Water Vapour	26	1.360 - 1.390	94.3	6.00	1.375
	27	6.535 - 6.895	254.6	1.16(240K)	6.715
	28	7.175 - 7.475	325.3	2.18(250K)	7.325
Cloud Properties	29	8.400 - 8.700	369.2	9.58(300K)	8.550
Ozone	30	9.580 - 9.880	300.6	3.69(250K)	9.730
Surface/Cloud Temperature	31	10.780 - 11.280	510.3	9.55(300K)	11.030
	32	11.770 - 12.270	493.5	8.94(300K)	12.020
Cloud Top Altitude	33	13.185 - 13.485	13.335	4.52(260K)	13.335
	34	13.485 - 13.785	13.635	3.76(250K)	13.635
	35	13.785 - 14.085	13.935	3.11(240K)	13.935
	36	14.085 - 14.385	14.235	2.08(220K)	14.235

[1] Bands 1 to 36 are in µm
[2] Bandwidth values are in nm
[3] Spectral radiance values are in Wm^{-2} μm^{-1} sr^{-1}
[4] Central wavelength values are in µm

In this study, the MODIS Terra data in MOD021KM format is used. These datasets were downloaded from the Level 1 and Atmosphere Archive and Distribution System (LAADS) website [9]. MOD021KM contains data in three forms: (1) Radiance (W $m^{-2}\mu m^{-1}sr^{-1}$) for the reflective bands (2) Radiance (W m^{-2} $\mu m^{-1}sr^{-1}$) for the emissive bands; and (3) Reflectance (dimensionless) for the reflective bands. The relationship between the TOA reflectance, ρ and TOA radiance ($Wm^{-2}\mu m^{-1}sr^{-1}$), L at the isotropic surface can be expressed as [4]:

$$L = \frac{E_\lambda \mu_s \rho}{\pi} \tag{1}$$

where E_λ is the mean exoatmospheric solar irradiance at TOA (W m^{-2} μm^{-1}), μ_s is $\cos(\theta_s)$ and π is a constant equal to ~3.14159 (unitless); θ_s is the solar zenith angle. The MODIS Level 1B also contains thermal data, which are recorded as TOA radiance, and can be converted to brightness temperature using the Planck function. Brightness temperature is defined as the temperature for an ideal black body with the observed radiance; it is the temperature a blackbody needs to have to emit radiation of the observed intensity at a given wavelength. From Planck's Law, the observed radiance is expressed as

$$L = \frac{2hc^2\lambda^{-5}}{\left(e^{\frac{hc}{k\lambda T}} - 1\right)} \tag{2}$$

where h is the Planck's constant (Js) equals to 6.626 x 10^{-34} Js, c is the speed of light in vacuum (ms^{-1}) equals to 3 x 10^8 ms^{-1}, k is the Boltzmann gas constant (JK^{-1}) equals to 1.3806503 × 10^{-23} JK^{-1}, λ is the band or detector centre wavelength (μm) and T is the brightness temperature (K). By inverting this formula, we can solve for brightness temperature, T:

$$T = \left(\frac{hc}{k\lambda}\right)\frac{1}{\ln\left(2hc^2\lambda^{-5}L^{-1} + 1\right)} \tag{3}$$

$$T = \left(\frac{c_2}{\lambda}\right).\frac{1}{\ln\left(\frac{c_1}{\lambda^5 L} + 1\right)} \tag{4}$$

where $c_2 = \frac{hc}{k} = 1.438 \times 10^4$ and $c_1 = 2hc^2 = 1.191 \times 10^8$.

The study area is Peninsular Malaysia, located within latitude $6^{o}47'$ N, longitude $88^{o}25'$ E (upper left), and latitude $1^{o}21'$ N, longitude $106^{o}20'$ E (lower right) that covers an area of about 140000 km^2.

3 Results and Discussion

The reflectance curves for the reflective MODIS bands are shown in Figure 2. The negative reflectances for cloud in bands 8 to 17 are caused by saturation problems and have been omitted. For the remaining bands, cloud over land has lower reflectances because it tends to be thinner than cloud over ocean. Brightness temperature curves for the thermal MODIS bands are shown in Figure 2 (b). These have the opposite trend to reflectance, with the brightness temperature of cloud over land being higher than cloud over the ocean. This is due to the fact that cloud over ocean is colder because it tends to be thicker than cloud over land [11]. Much larger standard deviations in reflectance and brightness temperature are observed for clouds over the land than ocean due to the larger variations in surface reflectivity and emissivity respectively. Land has much lower reflectances than cloud due to the much less reflective surface properties and lower altitudes. Land has higher reflectances and brightness temperatures than ocean due to the lesser energy absorption and higher temperature respectively. Ocean has lower standard deviations in reflectance and brightness temperature due to the much uniform spectral properties. Table 2 shows a set of cloud tests, which were formulated for use in this study. The set of tests was applied to multitemporal datasets of MODIS data. The same procedure such as that of the 30^{th} January 2004 dataset were applied to 24 other datasets from January 2004 to December 2005 at 0355 UTC (1155 LST). Figure 2 shows cloud masks generated for these datasets. It can be seen that cloud distribution changes dynamically with time; in overall, the cloud amount in 2005 seems to be more than 2004. This agrees with the fact that the total amount of rain received in 2005 was more than 2004 due to the effects of La Nina (wet spell) and El Nino (dry spell) respectively [8].

(a)

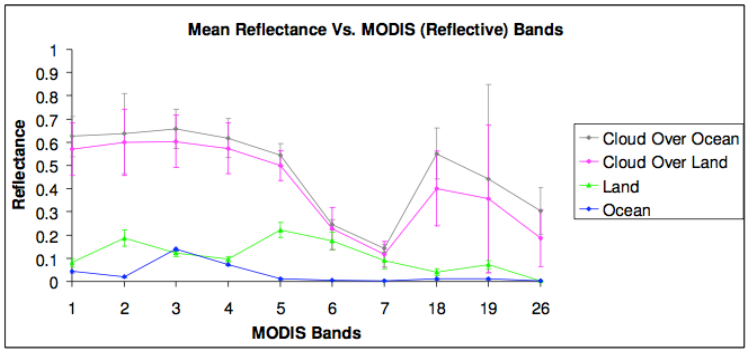

(b)

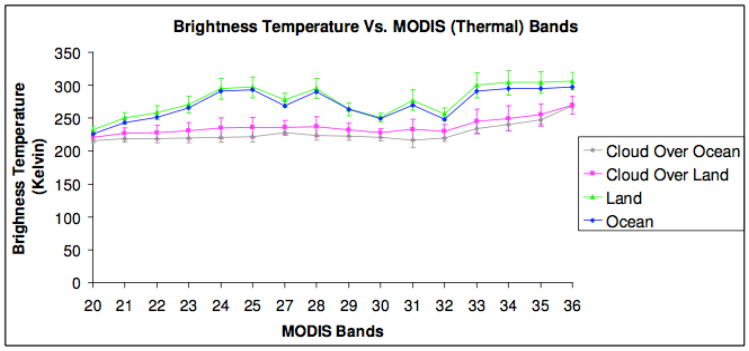

Fig. 1. (a) Reflectance of cloud over the ocean and cloud over the land relative to non-cloud features. Vertical bars indicate standard deviations; (b) Same as (a) but for brightness temperature.

Table 2: Cloud test, its function and the threshold used in the MODIS cloud mask for day-time detection over land.

Cloud criteria	Test (Subscript refers to MODIS band number)	Description	Threshold
Thick high clouds	BT_{35}	CO_2 slicing. Values smaller than threshold indicate ice cloud at middle and upper atmosphere	226 K
Thin high clouds	$BT_{31} - BT_{32}$	Values smaller than threshold indicate high cloud or cirrus cloud	2 K
Thick low clouds	$BT_{31} - BT_{22}$	Values smaller than threshold indicate low level water clouds	-11.0 K
Low clouds	R_1	Reflectance gross cloud test with vegetated land background. Values larger than threshold indicate cloud.	0.14
Thin high clouds	R_{26}	Values larger than threshold indicate thin cirrus cloud	0.03

Cloud trend within this period can be observed by plotting graph of area against the date of the datasets. Figure 3 shows cloud area against the date of the data from January 2004 to December 2005. It is noticeable that the 2005 datasets have more cloud than 2004 due to the effects of La Nina and El Nino respectively [8].

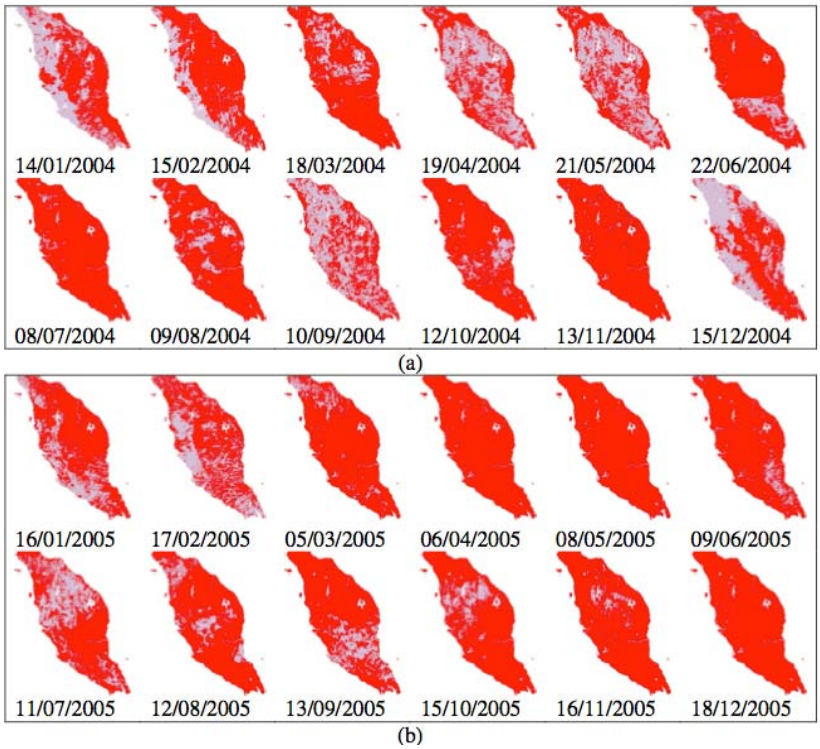

Fig. 2. Cloud masking for selected dates in (a) 2004, and (b) 2005; cloud pixels are masked red, while cloud-free and water body pixels are masked grey and white respectively.

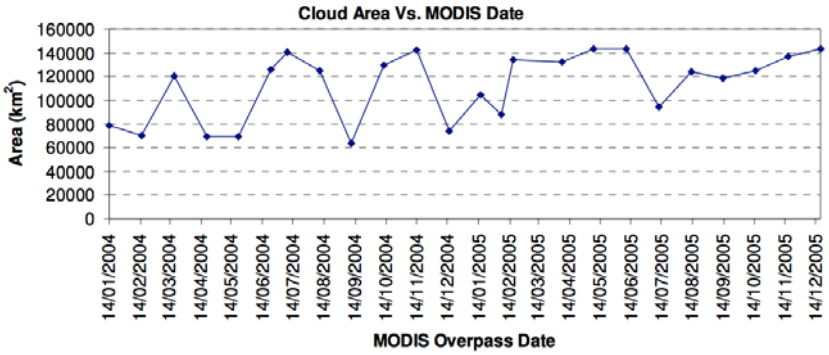

Fig. 3. Cloudy area versus different MODIS acquisition date from January 2004 to December 2005.

We further examine the areas where clouds are prone to form by classifying the cloud based on its frequency of occurrence. This was carried out by overlapping

the cloud masks in Figure 2 and then assigning colours to cloud pixels, based on the frequency of occurrence, for the year 2004 and 2005. Figure 4 shows the cloud area classified based on overlapping cloud pixels from the selected dates within 2004 and 2005; The colours are associated with the number of overlapping dates; non-cloud and water are masked grey and white respectively. The eastern parts of Malaysia seems to have more cloudy days than the western parts, in which consistence with the fact that the former is having more amount of annual rain than the later. It is also clear that the year 2005 is cloudier than 2004, in which is consistent with Figure 3, due to La Nina and En Nino respectively [8].

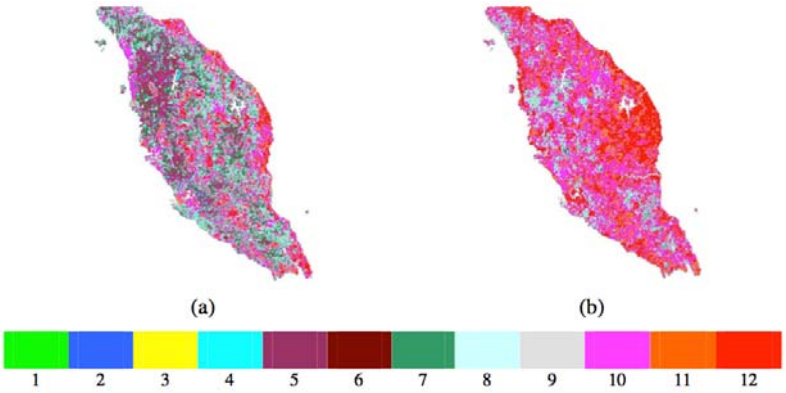

Fig. 4. Cloud area classified based on frequency of cloud occurrence from selected dates for (a) 2004 and (b) 2005. The colours are associated with the number of overlapping dates; non-cloud and water are masked grey and white respectively.

4 Conclusion

In this study, we investigated the spectral properties of cloud and carried out cloud detection and masking using spectral methods. Cloud was analysed based on measurements made from 36 MODIS bands ranging from visible to thermal wavelengths. Cloud detection and masking were first carried out individually using single date and then multi-dates of MODIS data. Multitemporal cloud analysis indicated that more cloudy days occured in the eastern parts of Malaysia, in which was consistence with the fact that more rain occured in the eastern than western parts of Malaysia.

References

[1] A. Ahmad, Analysis of Landsat 5 TM data of Malaysian land covers using ISODATA clustering technique, Proceedings of the 2012 IEEE Asia-Pacific Conference on Applied Electromagnetic (APACE 2012), (2012) , 92 – 97.

[2] A. Ahmad and M. Hashim, Determination of Haze Using NOAA-14 Satellite Data. Proceedings on The 23rd Asian Conference on Remote Sensing 2002 (ACRS 2002), (2012), in cd.

[3] A. Ahmad and S. Quegan, Analysis of maximum likelihood classification on multispectral data. Applied Mathematical Sciences, 6 (2012), 6425 – 6436.

[4] A. Ahmad and S. Quegan, Cloud masking for remotely sensed data using spectral and principal components analysis, Engineering, Technology & Applied Science Research (ETASR), 2 (2012), 221 – 225.

[5] A. Ahmad and S. Quegan, Comparative analysis of supervised and unsupervised classification on multispectral data. Applied Mathematical Sciences, 7(74) (2013), 3681 – 3694.

[6] B.-C. Gao, K.B. Heidebrecht and A. F. H. Goetz, Derivation of scaled surface reflectances from AVIRIS data. Remote Sensing of Environment, 44 (1993), 165 – 178.

[7] G.B. Franca and A.P. Cracknell, A simple cloud masking approach using NOAA AVHRR daytime data for tropical areas. International Journal of Remote Sensing, 9 (1995), 1697 – 1705.

[8] L. Wong, R. Venneker, S. Uhlenbrook, A. B. M. Jamil and Y. Zhou, Variability of rainfall in Peninsular Malaysia. Hydrology and Earth System Sciences Discussions, 6 (2009), 5471–5503.

[9] MODIS, 2007. Components of MODIS. Available at: http://modis.gsfc.nasa.gov/about/specifications.php [Accessed: 31 August 2013].

[10] R.W. Saunders and K.T. Kriebel, An improved method for detecting clear sky and cloudy radiances from AVHRR data. International Journal of Remote Sensing, 9 (1988), 123 –150.

[11] S. Ackerman, R. Frey, K. Strabala, Y. Liu, L. Gumley, B. Baum and P. Menzel, Discriminating clear-sky from cloud with MODIS - Algorithm theoretical basis document. Products: MOD35. ATBD Version 6.1, Madison: MODIS Cloud Mask Team, 2010.

[12] Wylie, W. P. Menzel and K.I. Strabala, Four years of global cirrus cloud statistics using HIRS. Journal of Climate, 7 (1994), 1972 – 1986.

Received: November 5, 2013